(A New Proposal to Jefferson Lab PAC-18)

Measurements of the Light Quark and Antiquark Distribution Ratios in the Nucleon Through Semi-Inclusive Reactions

X. Jiang (Co-Spokesperson) [a] , R. Ransome (Co-Spokesperson), S. Dieterich, G. Kumbartzki, R. Gilman, C. Glashausser, S. Strauch
Rutgers University, Piscataway, New Jersey, USA

J.-P. Chen, E. Chudakov, B. Wojtsekhowski, P. Degtiarenko, O. Hansen, K. de Jager, J. LeRose, R. Michaels, A. Saha
Jefferson Lab, Newport News, Virginia, USA

I. Danchev, R.Grima, R. Lindgren, V. Nelyubin, B. Norum, B. Sawatzky, A. Stolin, K. Wang
University of Virginia, Charlottesville, Virginia, USA

W. Bertozzi, S. Gilad, D.W. Higinbotham, R. Suleiman, Z. Zhou
Massachusetts Institute of Technology, Cambridge, Massachusetts, USA

J. Calarco and W. Hersman
University of New Hampshire, Durham, New Hampshire, USA

R. Hicks, A. Hotta, R. Miskimen, G. Peterson, J. Shaw
University of Massachusetts, Amherst, Massachusetts, USA

S. Churchwell
Duke University, Durham, North Carolina ,USA

M. Jones
University of Maryland, College Park, Maryland, USA

T.-H. Chang, A. Nathan
University of Illinois , Urbana-Champaign, Illinois, USA

We propose to measure the semi-inclusive $(e, e'\pi^+)$ and $(e, e'\pi^-)$ yield ratios on hydrogen and deuterium in the kinematic range of $0.1 < x < 0.4$, $1.0 < Q^2 < 4.0$ GeV^2, and $7.0 < W^2 < 9.5$ GeV^2 in JLab Hall-A with a 6 GeV electron beam. In the case that a generalized form of factorization between the virtual photon-quark hard scattering process and quark hadronization applies, the charge pion yield ratio can be easily related to $(d+\bar{d})/(u+\bar{u})$ and $(d-\bar{d})/(u-\bar{u})$. We propose to determine the above ratios to 1.25% and 0.5% statistical accuracy, respectively, to provide strong constrains on the quark distribution functions. This experiment will also allow us to determine if a significant asymmetry exists between the $\bar{d}$ and $\bar{u}$ distributions.

[a] Contact person. Email: jiang@jlab.org

1 Introduction: Light Quark and Antiquark Distributions

Since the discovery of the quark substructure of the nucleon many experiments have been devoted to measuring and understanding the quark momentum distributions. Although we now have a fairly good understanding of valence quark properties, the distributions of the sea quarks and antiquarks which accompany the valence quarks are still somewhat uncertain. Recent measurements have indicated that there may be more structure in the sea distributions than previously expected. Approaching this question via a new reaction mechanism is the basis of this proposal.

1.1 Gottfried sum rule violation, NMC results.

The first indication of the inequality of $\bar{u}(x)$ and $\bar{d}(x)$ came from measurements of the Gottfried integral [1] which is defined as:

$$I_G = \int_0^1 \left[F_2^p(x,Q^2) - F_2^n(x,Q^2)\right] \frac{dx}{x} \tag{1}$$

where F_2^p and F_2^n are the proton and neutron structure functions measured in deep inelastic scattering experiments. In terms of the valence and sea quark distributions of the proton, under the assumption of isospin symmetry, I_G can be expressed as:

$$I_G = \frac{1}{3}\int_0^1 \left[u_v(x,Q^2) - d_v(x,Q^2)\right] dx + \frac{2}{3}\int_0^1 \left[\bar{u}(x,Q^2) - \bar{d}(x,Q^2)\right] dx \tag{2}$$

A flavor-symmetric nucleon sea ($\bar{u}(x) = \bar{d}(x)$) would lead to $I_G = 1/3$, the Gottfried sum rule [1]. Measurements by the New Muon Collaboration (NMC) [2] determined that $\int_{0.004}^{0.8} [F_2^p(x) - F_2^n(x)]/x \; dx = 0.221 \pm 0.021$ at $Q^2 = 4$ GeV^2. Extrapolating to x=0 through the unmeasured small-x region, they projected that $I_G = 0.235 \pm 0.026$, significantly below 1/3. Specifically, the NMC result implies that $\int_0^1 \left[\bar{d}(x) - \bar{u}(x)\right] dx = 0.148 \pm 0.039$. While no known symmetry requires $\bar{u}$ to equal $\bar{d}$, a large $\bar{d}/\bar{u}$ asymmetry was not anticipated. Many ideas such as Pauli blocking and pion clouds have been proposed to explain such a flavor asymmetry in the sea [3]. Two methods have been suggested to measure its x-dependence: the Drell-Yan process [4] and the semi-inclusive deep inelastic scattering [5].

1.2 Light antiquark asymmetry in the nucleon sea.

Recently, Fermilab experiment E866 reported measurements of the yield ratio of Drell-Yan muon pairs from an 800 GeV/c proton beam incident on hydrogen and deuterium [6]. The data suggested a significantly asymmetric light-quark sea distribution over an appreciable range in x; the asymmetry peaked around $x = 0.13$. The ratio of the Drell-Yan cross section per nucleon for p+d to that of p+p at Q^2=50.0 GeV^2 is shown in Fig. 1. Assuming isospin symmetry, the Drell-Yan ratio can be

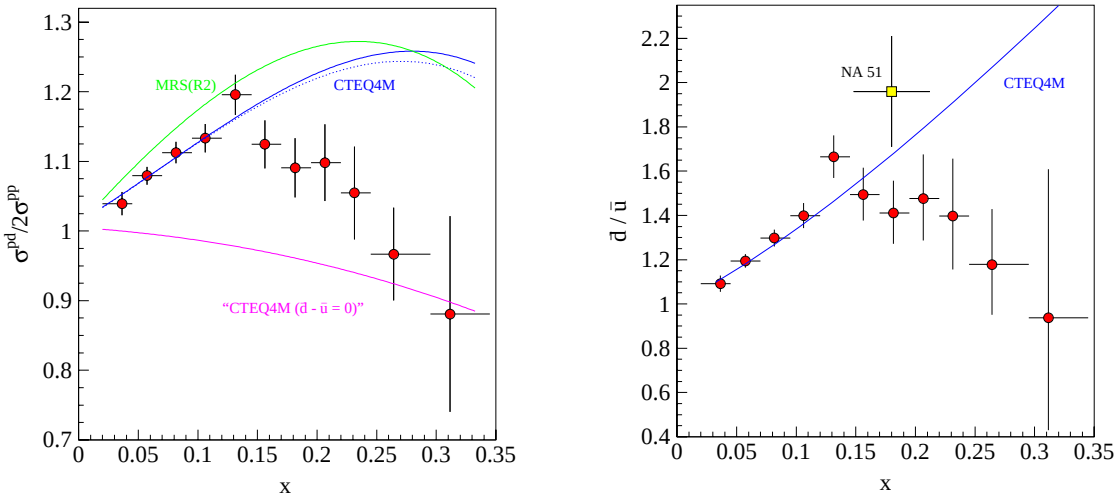

Figure 1: Fermilab E866 results. The left plot shows ratio of $\sigma^{pd}/2\sigma^{pp}$ of Drell-Yan cross sections vs the target quark momentum fraction x. The lower dotted line shows the CTEQ4M curve while taking $\bar{d} - \bar{u} = 0$. The right plot shows the ratio of $\bar{d}/\bar{u}$ as a function of x. The result from CERN experiment NA51 is shown as an open box.

expressed as:

$$\frac{\sigma^{pd}}{2\sigma^{pp}} \approx \frac{1}{2} \frac{(1 + \frac{1}{4}\frac{d_1}{u_1})}{(1 + \frac{1}{4}\frac{d_1}{u_1}\frac{\bar{d}_2}{\bar{u}_2})} \left(1 + \frac{\bar{d}_2}{\bar{u}_2}\right), \tag{3}$$

where the subscript 1 (or 2) indicates the target (or beam) quark. Assuming $\bar{d} + \bar{u}$ distributions are accurate in global fits of quark distributions, such as CTEQ4M [7] (and MRST(R2) [8]), E866 extracted $\bar{d}/\bar{u}$ from the measured Drell-Yan ratio, as shown in Fig. 1.

Furthermore, based on the E866 data and the CTEQ4M global-fit values of $(\bar{d}+\bar{u})$, Peng *et al.* [9] concluded that $\int_0^1 \left[\bar{d}(x) - \bar{u}(x)\right] dx = 0.100 \pm 0.007 \pm 0.017$.

The apparent difference between the NMC and E866 results for the $\bar{d} - \bar{u}$ raises the question of the compatibility of the two measurements. Questions were raised on the reliability of existing parton distribution functions, for example, in the region of $x > 0.23$. Unfortunately, due to limited statistics, the uncertainty of the E866 data is larger in this region. In the region of $0.156 < x < 0.312$, the accuracy of E866 $\bar{d}/\bar{u}$ results also relies on the knowledge of $\bar{d} + \bar{u}$ from earlier experimental data. Therefore, independent confirmation of sea quark distributions from different reaction channels could help to clarify the issue. The semi-inclusive $(e, e'\pi^{\pm})$ reaction is one natural choice because of the advantage in flavor tagging.

1.3 Semi-inclusive pion production in electron scattering.

Semi-inclusive reactions in electron scattering can be used as a tool to study the density distributions of valence quarks as well as sea quarks. Specifically, pion

electro-production on hydrogen and deuterium offers a unique probe of light quark and anti-quark distributions. At high enough energy transfer, the Independent Factorization between the virtual photon-quark hard scattering process and the hadronization of the struck quark implies that:

$$Y^{\pi^\pm}(x,z) \propto \sum_i e_i^2 \left[q_i(x) D_{q_i}^{\pi^\pm}(z) + \bar{q}_i(x) D_{\bar{q}_i}^{\pi^\pm}(z) \right], \tag{4}$$

where $Y^{\pi^\pm}(x,z)$ is the π^+ (π^-) yield in deep-inelastic scattering, $z = E^\pi/\nu$ is the fraction of the virtual photon energy carried by the pion, e_i is the quark charge, $q_i(x)$ and $\bar{q}_i(x)$ are the density distributions of quark and anti-quark of flavor i. The fragmentation functions $D_{q_i}^{\pi^\pm}(z)$ represent the probability that a quark of flavor i fragments into a charged pion. Assuming isospin symmetry and charge conjugation invariance, the number of light quark fragmentation functions is reduced to two type: the favored (D^+) and the unfavored (D^-) fragmentation functions:

$$D^+ \equiv D_u^{\pi^+} = D_d^{\pi^-} = D_{\bar{u}}^{\pi^-} = D_{\bar{d}}^{\pi^+}, \tag{5}$$

$$D^- \equiv D_u^{\pi^-} = D_d^{\pi^+} = D_{\bar{u}}^{\pi^+} = D_{\bar{d}}^{\pi^-}. \tag{6}$$

The HERMES collaboration recently published data on the ratio of $(\bar{d}-\bar{u})/(u-d)$ in the kinematic range of $0.02 < x < 0.3$ and $1 < Q^2 < 10$ GeV^2. Through measurements of the yield ratio

$$r(x,z) = \frac{Y_p^{\pi^-}(x,z) - Y_n^{\pi^-}(x,z)}{Y_p^{\pi^+}(x,z) - Y_n^{\pi^+}(x,z)}, \tag{7}$$

the flavor asymmetry was determined as:

$$\frac{\bar{d}(x) - \bar{u}(x)}{u(x) - d(x)} = \frac{J(z)[1 - r(x,z)] - [1 + r(x,z)]}{J(z)[1 - r(x,z)] + [1 + r(x,z)]}, \tag{8}$$

in which $J(z) = \frac{3}{5}\left(\frac{1+D'(z)}{1-D'(z)}\right)$ with $D'(z) = D_u^{\pi^-}/D_u^{\pi^+}$. The HERMES data are shown in Fig. 2, with the ratio $(\bar{d} - \bar{u})/(u - d)$ in the top plot and $(\bar{d} - \bar{u})$ in the lower plot in which the values of $(u - d)$ were taken from the GRV-94 leading order parameterization [10]. With large statistical uncertainties, the HERMES data agree with E866 results, even though the Q^2 of the two experiments differs by a factor of about 20.

To demonstrate the evidence of factorization, HERMES also measured the ratio of $(\bar{d} - \bar{u})/(u - d)$ as a function of z as shown in Fig. 3 for five x-bins. Since no indication of z dependence was observed, the data are consistent with the form of factorization as in Eq. 4. We note that this evidence of factorization occurred at $1.33 < Q^2 < 4.88$ GeV^2, with the requirement that the invariant mass $W^2 > 4.0$ GeV^2, which is accessible at Jefferson Lab with a beam energy of 6.0 GeV.

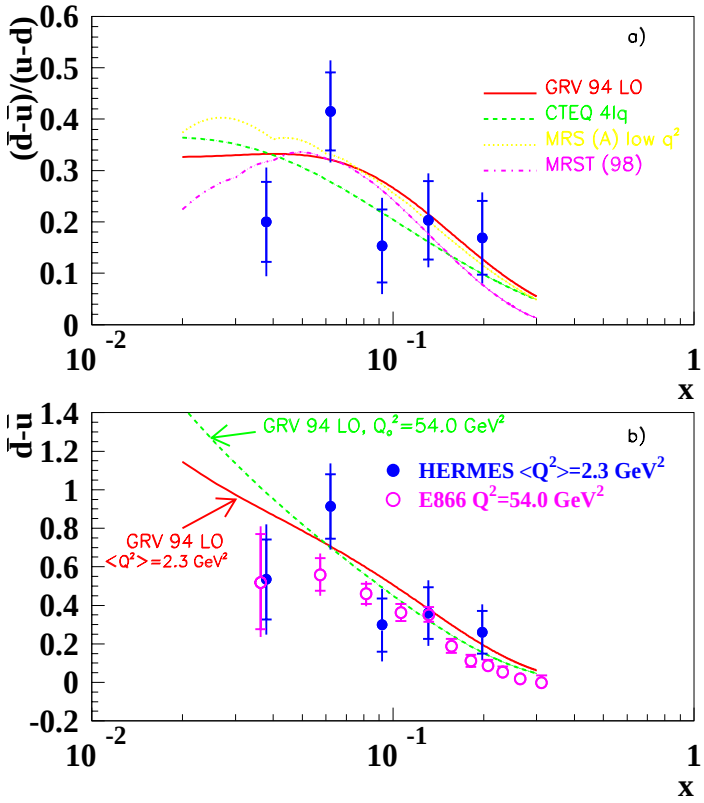

Figure 2: HERMES results of $(\bar{d}-\bar{u})/(u-d)$ in (a) and $\bar{d}-\bar{u}$ in (b) as a function of x. The open circles represent the E866 determination of $\bar{d}-\bar{u}$ at Q^2=54.0 GeV^2.

1.4 Semi-inclusive reactions at JLab Hall-A.

In this proposal, we seek to determine the semi-inclusive π^+ and π^- yield on proton and deuteron targets with high statistical accuracy in the kinematic range of $0.1 < x < 0.4$, $1.0 < Q^2 < 4.0$ GeV^2 , and $7.0 < W^2 < 9.5$ GeV^2. The invariant mass of the hadron system without the detected pion will be in the range of $3.5 < W'^2 < 6.1$ GeV^2. Through measurements at different z, we hope to reproduce the z-independence of the yield ratios as reported by HERMES in order to demonstrate the evidence of factorization. In the case that a generalized factorization applies between the virtual photon-quark hard scattering process and the hadronization of the struck quark, precise measurements of pion yield ratios can be used as independent constraints in the determination of valence quark and sea quark distributions.

Assuming isospin symmetry and charge conjugation (i.e. $u_p(x) = d_n(x)$, $d_p(x) = u_n(x)$, $\bar{u}_p(x) = \bar{d}_n(x)$, $\bar{d}_p(x) = \bar{u}_n(x)$) and neglecting heavy quark contributions, under the condition of Independent Factorization of Eq. 4, the yield of $\pi^\pm$ in deep

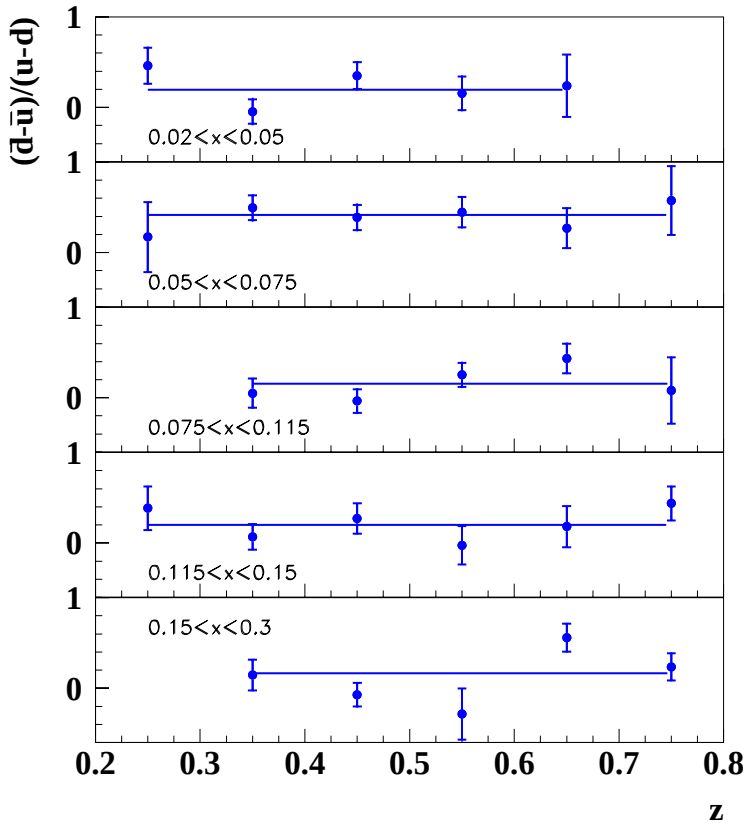

Figure 3: HERMES evidence of factorization. The distribution of $(\bar{d}-\bar{u})/(u-d)$ as a function of z in five bins of x.

inelastic scattering on the proton and neutron can be expressed as:

$$Y_p^{\pi^+}(x,z) = A\left(4u(x)D^+(z) + d(x)D^-(z) + 4\bar{u}(x)D^-(z) + \bar{d}(x)D^+(z)\right), \quad (9)$$
$$Y_p^{\pi^-}(x,z) = A\left(4u(x)D^-(z) + d(x)D^+(z) + 4\bar{u}(x)D^+(z) + \bar{d}(x)D^-(z)\right),$$
$$Y_n^{\pi^+}(x,z) = A\left(4d(x)D^+(z) + u(x)D^-(z) + 4\bar{d}(x)D^-(z) + \bar{u}(x)D^+(z)\right),$$
$$Y_n^{\pi^-}(x,z) = A\left(4d(x)D^-(z) + u(x)D^+(z) + 4\bar{d}(x)D^+(z) + \bar{u}(x)D^-(z)\right).$$

where A is a common kinematic factor.

If four independent yields ($Y_p^{\pi^+}, Y_p^{\pi^-}, Y_n^{\pi^+}$ and $Y_n^{\pi^-}$) are measured, ratios of yields can be formed in which the fragmentation functions cancel each other:

$$t_1(x) = \frac{Y_p^{\pi^+}(x,z) + Y_p^{\pi^-}(x,z)}{Y_n^{\pi^+}(x,z) + Y_n^{\pi^-}(x,z)} = \frac{4u(x) + d(x) + 4\bar{u}(x) + \bar{d}(x)}{4d(x) + u(x) + 4\bar{d}(x) + \bar{u}(x)}, \quad (10)$$

$$t_2(x) = \frac{Y_p^{\pi^+}(x,z) - Y_p^{\pi^-}(x,z)}{Y_n^{\pi^+}(x,z) - Y_n^{\pi^-}(x,z)} = \frac{4u(x) - d(x) - 4\bar{u}(x) + \bar{d}(x)}{4d(x) - u(x) - 4\bar{d}(x) + \bar{u}(x)}. \quad (11)$$

Or simply as:

$$r_1(x) = \frac{4 - t_1(x)}{4t_1(x) - 1} = \frac{d(x) + \bar{d}(x)}{u(x) + \bar{u}(x)} = \frac{d_v(x) + 2\bar{d}(x)}{u_v(x) + 2\bar{u}(x)} \tag{12}$$

and

$$r_2(x) = \frac{4 + t_2(x)}{4t_2(x) + 1} = \frac{d(x) - \bar{d}(x)}{u(x) - \bar{u}(x)} = \frac{d_v(x)}{u_v(x)}, \tag{13}$$

in which $u_v(x) = u(x) - \bar{u}(x)$ and $d_v(x) = d(x) - \bar{d}(x)$.

A different yield ratio can be taken as:

$$\begin{aligned} r_3(x) &= \frac{25}{9} \cdot \frac{(Y_p^{\pi^+} + Y_n^{\pi^+}) - (Y_p^{\pi^-} + Y_n^{\pi^-})}{(Y_p^{\pi^+} + Y_n^{\pi^+}) + (Y_p^{\pi^-} + Y_n^{\pi^-})} \cdot \frac{(Y_p^{\pi^+} - Y_n^{\pi^+}) + (Y_p^{\pi^-} - Y_n^{\pi^-})}{(Y_p^{\pi^+} - Y_n^{\pi^+}) - (Y_p^{\pi^-} - Y_n^{\pi^-})} \\ &= \frac{u + d - \bar{u} - \bar{d}}{u + d + \bar{u} + \bar{d}} \cdot \frac{u - d + \bar{u} - \bar{d}}{u - d - \bar{u} + \bar{d}} = \frac{u_v + d_v}{u_v - d_v} \cdot \frac{u_v - d_v + 2\bar{u} - 2\bar{d}}{u_v + d_v + 2\bar{u} + 2\bar{d}}. \end{aligned} \tag{14}$$

In the above formalism, we've omitted the notation of Q^2 dependence of the ratios and distribution functions.

Clearly, observation of $r_1 \neq r_2$ would serve as direct evidence of a non-vanishing sea-quark distribution, since without the sea-quarks, one would expect $r_1 \equiv r_2$ and $r_3 \equiv 1$. Furthermore, precise measurements of r_1 and r_2 at different x and Q^2 will provide strong and independent constraints on the parton distribution functions, especially in the high-x region where existing data lack accuracy.

We note that the Independent Factorization condition of Eq. 4 is not an absolute requirement in the cancellation of fragmentation functions in the derivation of Eq. 10 and 11. A much more relaxed form of factorization can be tolerated. The fragmentation functions can take a more general form, for example $D = D(\nu, Q^2, z)$. As long as the fragmentation functions are not explicitly depend on the quark distributions, and as long as isospin symmetry and charge conjugation hold between different fragmentation functions, the ratios r_1, r_2, and r_3 will be independent of z and the fragmentation functions. Later on, we will refer to this relaxed form of factorization as the Generalized Factorization Condition. A clear signature of the onset of the generalized factorization will be the apparent scaling behavior of r_1 and r_2 at different values of z. In this experiment, we propose to measure r_1 and r_2 to statistical accuracies of 1.25% and 0.50%, respectively, in order to clearly demonstrate the validity of generalized factorization at each kinematic setting. We also note that exact knowledge about the fragmentation functions is not needed in this experiment because they cancel out in the yield ratios. The predicted values of r_1 and r_2 at Q^2=2.23 GeV^2 are plotted in Fig. 4 from CTEQ5M predictions. The sensitivity of r_1 and r_2 to different values of $\bar{d}/\bar{u}$ ratios are also shown while the value of $\bar{d} + \bar{u}$ is fixed by CTEQ5M.

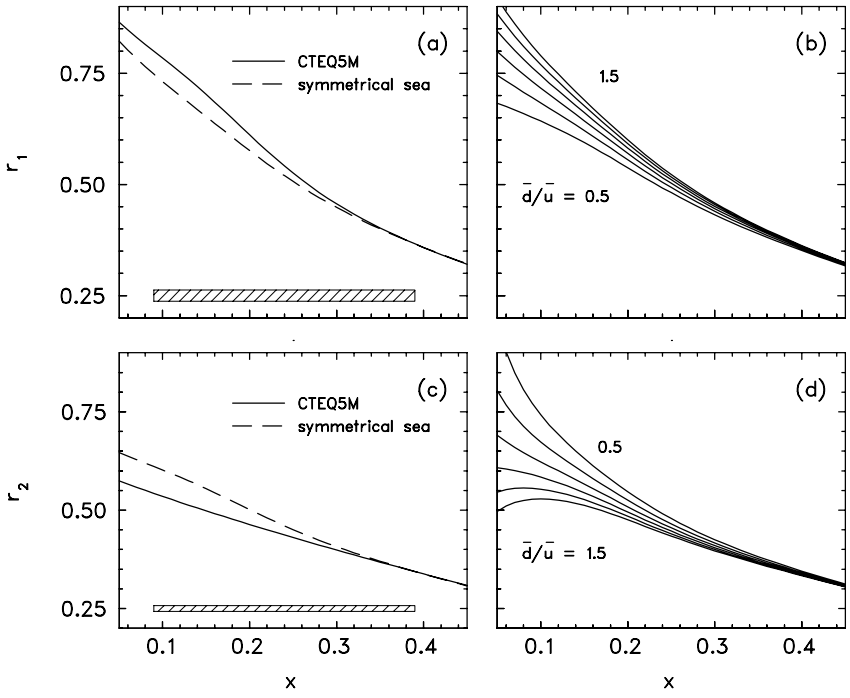

Figure 4: The ratio of r_1 and r_2 at Q^2=2.23 GeV^2 from CTEQ5M predictions. The dashed lines represent the value when $\bar{d} - \bar{u} = 0$ is forced while $\bar{d} + \bar{u}$ is fixed by CTEQ5M. The shaded area represent the sensitivity corresponding to a measurement of 1.25 % (0.5 %) error on r_1 (r_2). In plots (b) and (d) six different $\bar{d}/\bar{u}$ values uniformly spread from 0.5 to 1.5 are assumed in the CTEQ5M predictions.

We plan to extract the neutron yield from the deuteron and hydrogen yield difference. Nuclear binding effects and corrections due to Fermi motion are expected to be small in the region of $0.1 < x < 0.4$. [11]. Under the assumption that $Y_D^{\pi^\pm} = Y_n^{\pi^\pm} + Y_p^{\pi^\pm}$, r_1 and r_2 can be expressed as:

$$r_1 = -1 + \frac{3}{5\rho_1 - 1}, \tag{15}$$

$$r_2 = -1 + \frac{5}{3\rho_2 + 1}, \tag{16}$$

where

$$\rho_1 = \frac{Y_p^{\pi^+} + Y_p^{\pi^-}}{Y_D^{\pi^+} + Y_D^{\pi^-}}, \tag{17}$$

$$\rho_2 = \frac{Y_p^{\pi^+} - Y_p^{\pi^-}}{Y_D^{\pi^+} - Y_D^{\pi^-}} \tag{18}$$

are measured directly from experiment. A different combination of ρ_1 and ρ_2 gives r_3 as :

$$r_3 = \frac{25}{9} \cdot \frac{2\rho_1 - 1}{2\rho_2 - 1}. \tag{19}$$

The measurement uncertainties $\delta\rho_2$ and $\delta\rho_2$ propagate to r_1 and r_2 through:

$$\delta r_1 = \frac{5}{3}(1+r_1)^2\delta\rho_1, \qquad (20)$$
$$\delta r_2 = \frac{3}{5}(1+r_2)^2\delta\rho_2.$$

Thus, to improve the precision on r_1 and r_2 measurements one needs to minimize $\delta\rho_1$ and $\delta\rho_2$. This implies that one should measure the yield from hydrogen and deuterium with similar relative accuracy and measure the π^+ and π^- yields with similar absolute accuracy for each target.

2 The Experiment

2.1 Experimental goal.

By studying deep inelastic semi-inclusive $(e, e'\pi^{\pm})$ reaction on hydrogen and deuterium at the highest possible W^2 and W'^2 available to JLab at 6 GeV, we plan to measure the yield ratios r_1 and r_2 to high statistical accuracy (1.25% and 0.5%) in order to extract light quark and anti-quark distribution ratios in the nucleon. By examining the z-dependence of these ratios, we expect to reproduce the HERMES observation of factorization with much higher precision.

The planned experiment will use one Hall-A HRS spectrometer with the septum magnet at 6° as the hadron arm. The electron arm will be based on the Big Bite dipole magnet with a detector package assembled mostly from existing equipments.

2.2 Kinematics choice

The kinematic variables are defined in Fig. 5. We always use a beam energy of E=6.0 GeV. E′ and θ_e are the energy and angle of the scattered electron, p_π and θ_π are the momentum and lab angle of the detected pion, $z = E_\pi/\nu$. W^2 is the invariant mass squared of the whole hadron system and W'^2 is the invariant mass squared of the hadron system without the detected pion.

We chose to cover the region of $0.1 < x < 0.4$ and the highest possible W^2 with 6 GeV beam in order to be as far as possible into the deep inelastic region. We also chose to detect the fragmentation products directly along the momentum transfer with $35\% \sim 65\%$ of total energy transfer to favor the current fragmentation regime rather than the target fragmentation regime. The W'^2 are also chosen to be the highest possible (3.5 GeV^2 to 6.1 GeV^2) to avoid contributions from resonance structures. These choices make the direction of $\vec{q}$ very close to the beam line, thus, the use of septum magnet is necessary. Because the design of the septum magnet moves the interaction points 80 cm upstream of the regular target location, the other HRS spectrometer cannot be used at an angle larger than 12.3°. We plan to assemble an electron arm spectrometer using the existing Big Bite dipole magnet

Table 1: Summary of central values of kinematic settings at beam energy $E = 6.0$ GeV. E$'$(in GeV) and θ_e(in degree) are electron arm momentum and angle, θ_q(in degrees) indicates the direction of $\vec{q}$, θ_π(in degrees) is the hadron arm angle (fixed at 6°), P_π(in GeV/c) is the hadron arm momentum. W^2 (in GeV^2) is the invariant mass square of the hadron system, W'^2 (in GeV^2) is the invariant mass square of the hadron system without the detected pion. Each kinematic setting contains (e,e$'\pi^+$) and (e,e$'\pi^-$) runs on hydrogen and deuterium targets.

Label	E$'$	θ_e	ν	$\langle x \rangle$	W^2	Q^2	$\mid \vec{q} \mid$	θ_q	θ_π	z	P_π	W'^2
	1.05	25.50	4.95	.13	8.94	1.23	5.07	5.11	6.00			
K1a										0.35	1.75	6.12
K1b										0.41	2.03	5.63
K1c										0.47	2.33	5.15
K1d										0.53	2.62	4.66
K1e										0.59	2.92	4.18
K1f										0.65	3.22	3.69
	0.90	37.50	5.10	.23	8.22	2.23	5.31	5.92	6.00			
K2a										0.35	1.78	5.63
K2b										0.41	2.09	5.19
K2c										0.47	2.40	4.75
K2d										0.53	2.70	4.31
K2e										0.59	3.01	3.86
K2f										0.65	3.31	3.45
	0.60	59.50	5.40	.35	7.47	3.55	5.72	5.19	6.00			
K3a										0.35	1.89	5.13
K3b										0.41	2.21	4.73
K3c										0.47	2.54	4.32

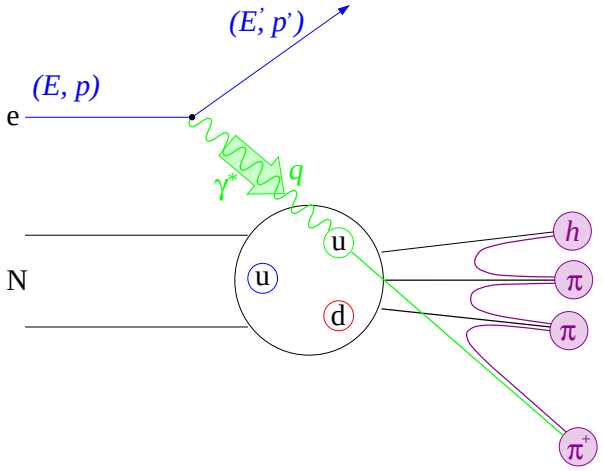

Figure 5: Diagram of (e,e'π) reaction on nucleon.

and a modified detector package based on the existing Real Compton Scattering experiment [12] detector setup.

Because of the finite acceptance of the planned electron-arm Big-Bite spectrometer ($\Delta\Omega = 10$ msr, $\Delta P/P = \pm 20\%$), a wider kinematic region is covered. The coverage in the (x, Q^2) plane is shown in Fig. 6, and the coverage in the (x, W^2) plane is shown in Fig. 7. The data will have enough statistics to allow six x-bins in Kinematics-1 and -2 and three x-bins in Kinematics-3. In principle, the Big Bite spectrometer in the planned configuration can provide a even larger momentum acceptance, but we took a conservative approach in estimating count rates.

Although the absolute efficiencies of pion detection will cancel in the yield ratios, changes in relative efficiencies, especially between π^+ and π^- measurements could introduce systematic errors. At each electron-arm kinematics, several hadron arm momentum settings are planned. They overlap each other by 3% in momentum bite to provide self-consistency monitoring in pion detection efficiencies.

Fig. 8 shows the Hall-A floor configuration for Kinematics-1, with the Big Bite dipole magnet located 2.5 meters away from the target at an angle of 25.5°. Well-collimated shielding is planned in front of the magnet to reduce background. Shielding between the detector package and the beam dump are also required.

2.3 Spectrometers and detectors

Hadron Arm Spectrometer and Detectors

The hadron arm HRS spectrometer will be in its standard configuration with a threshold gas Cherenkov and an aerogel Cherenkov (with n=1.015, and proton threshold of 5.5 GeV). Two layers of lead glass shower counters at the very end of the detector package are also needed to provide additional π/e separation. We

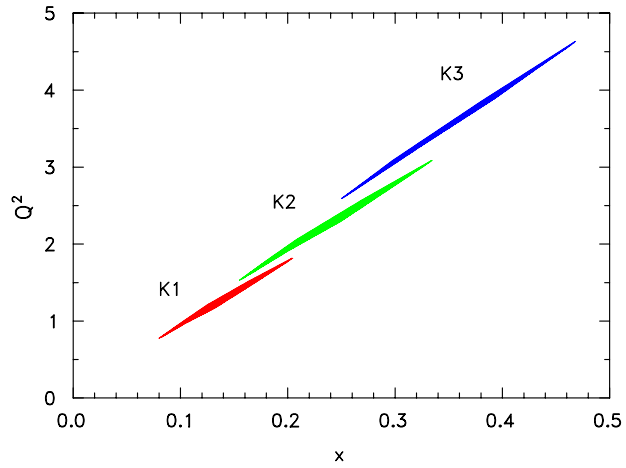

Figure 6: Kinematic coverage of (x, Q^2).

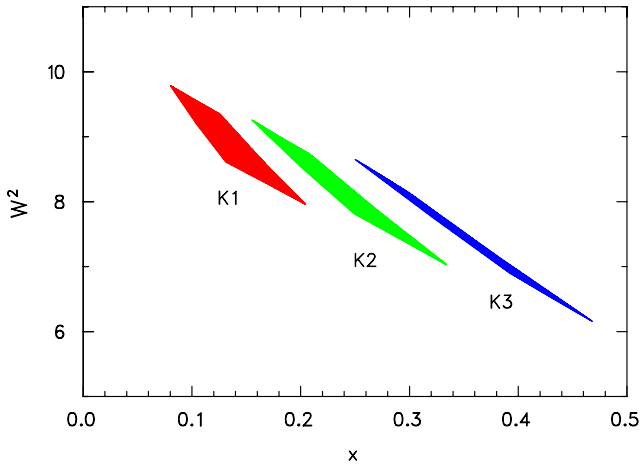

Figure 7: Kinematic coverage of (x, W^2).

require the gas cherenkov signal to be included in the trigger as an online veto to e^+ and e^-.

The Electron Arm Spectrometer and Detectors

We plan to put the Big Bite dipole 2.5 meters away from the target as a deflection magnet for the electron arm. The electron arm configuration presented here is based on the following considerations:

- The background decreases quickly with increasing particle momentum. The bending angle should be as large as the detector size allows and the detector should not see the target directly.
- To provide particle ID and good pion rejection, well segmented shower detectors should be used. The existing Real Compton Scattering (RCS) calorimeter is a good choice.

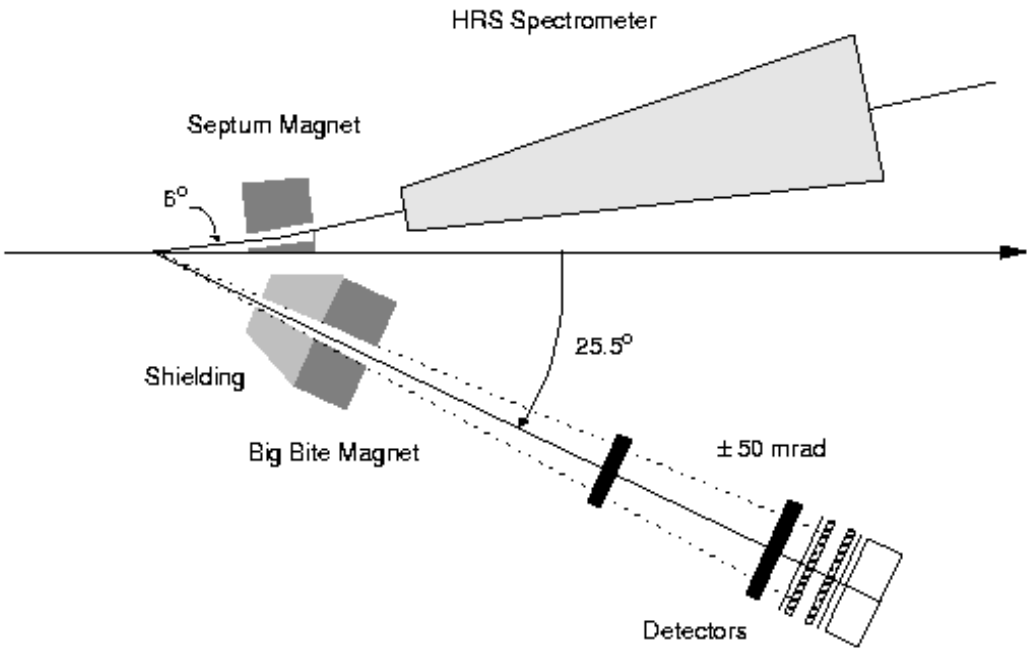

Figure 8: Experimental floor plan of kinematics-1.

- Segmented scintillators can be used to reduce events from background.
- An additional Cherenkov counter would help in eliminating pion contamination. Aerogel Cherenkov counters with $n = 1.008$ allow compact design with reasonable segmentation.
- Reconstruction of the vertex in target gives a large reduction factor on accidental events. Reasonable target reconstruction can be done with Big Bite which has simple optics. Additional proportional wire chambers need to be installed.
- Knowledge of the electron energy with the calorimeter allows the trajectory of electron to be reconstructed even with multiple hit events in the wire chamber.

A GEANT Monte Carlo simulation was done to guide the design of the electron arm detector package. Fig. 9 shows the simulation of negative particles passing through the well-collimated Big Bite magnet. Based on the simulation, the location of the RCS calorimeter is chosen to be 7.5 meters away from the magnet.

Under the above configuration, reasonable acceptance ($\sim 60\%$) can be achieved over a momentum bite of at least $\pm 20\%$. Fig. 10 shows simulation result of the Big Bite momentum acceptance.

Fig. 11 shows a schematic view of the detector package design. Separated by 2.5 meters, front(M1) and rear(M2) MWPC will have three planes (U1, V1, W1) with

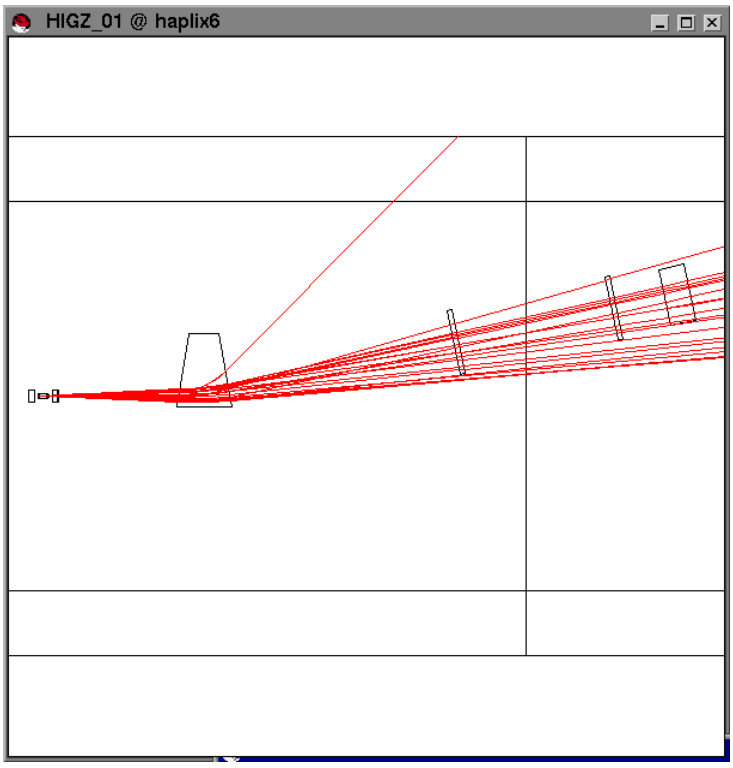

Figure 9: GEANT simulation of negatively charged particles passing through Big Bite magnet. The locations of two wire chambers and the RCS lead glass array are also shown. Positively charged and neutral particles are outside the view of detectors.

wire spacing of 2.0 mm. Helium bags will be put inside the magnet and between two wire chambers to reduce multiple scattering. The angular resolution will be about 1 mrad, and the momentum resolution will be better than 1.0%. Two layers of scintillator (S1, S2) and two Aerogel Cherenkov (A1, and A2) counters will be segmented into 8 sections each. Their orientation will be alternated between two different directions. Scintillator time resolution of 0.25 ns is expected. The existing RCS lead glass calorimeter (PbG) has 704 blocks with the size (40 by 40 by 400 mm).

There are a large number of available components for this detector package. The RCS Lead Glass Calorimeter and its DAQ are under construction and development for experiment E99-114. It is the most expensive part of the detector. Aerogel Cherenkov counters can be assembled from components of existing counters in Hall A except the aerogel material ($n = 1.008$). 5-inch PMTs are available from Hall A Cherenkov counters. We are discussing with MIT/Bates the possibility of borrowing the MWPC from Bates FPP system and instrument it with a PICO4 readout which is available in Hall A. These MWPC has dimensions of 37x71 and 88x142 cm which fit perfectly with the proposed geometry. We will need to add third plane to the MWPC chamber for tracking improvement.

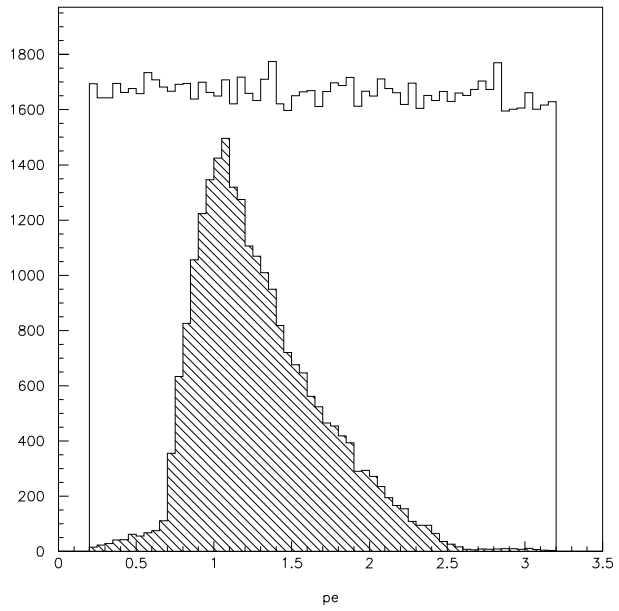

Figure 10: Big Bite momentum acceptance at 1.0 GeV setting. The histogram shows random electron rays (with energy pe) starting from the target with $\Delta\theta_{hor} = \pm 50$ mrad and $\Delta\theta_{ver} = \pm 50$ mrad. The shaded area represents particles accepted by the detector package.

2.4 Background rates and accidental coincidence rates.

Single electron rates in each arm are estimated using deep inelastic scattering cross sections (see next section). Single proton and pion rates are estimated by a code of J.S. O'Connell and J.W. Lightbody, Jr. [13]

For the hadron arm at 6°, the electron singles rate in the worst case is in the order of 100 kHz, positron rates are certainly less than the electron rates. Pion singles rates are less than 30 kHz, and proton singles rates are of the order of 2 kHz in the worst case. The combination of the threshold gas Cherenkov and two layers of lead-glass shower counters should provide sufficient e^-/π^- and e^+/π^+ separation. For the electron arm, in the worst case (at 25.5° and 1.0 GeV), the electron singles rates should be less than 30 kHz, and the π^- rates less than 150 kHz. The π^-/e^- ratio will not exceed 10:1 on the electron arm throughout the experiment. Nevertheless, we introduced two well-segmented aerogel Cherenkov counters in the electron arm detector package design to further reduce the possibility of pion contamination. Combined with the well segmented RCS lead-glass array $e^-\pi^-$ separation should not be an issue in the electron arm.

The trajectory corrected time-of-flight resolution is expected to be better than 1.0 ns. The worst signal-to-noise ratio will occur at settings K1a - K1d, assuming a 2.0 ns coincident time window, the accidental rates of $(e^-\pi^-)$ or $(e^-\pi^+)$ could reach the few Hz level while the true coincident rates are above 20 Hz. Since both arms

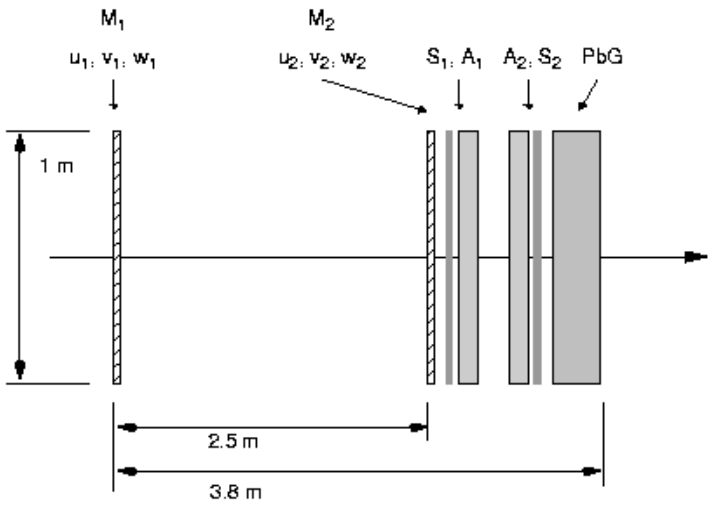

Figure 11: Electron arm detector configuration.

have an interaction point resolution of at least 2.0 cm along the beam, an additional accidental reduction factor of 7.5 can be easily achieved for a 15 cm long target. Therefore, the signal-to-noise ratio will be higher than 10:1 in the worst case.

3 Count Rate Estimate and Beam Time Request

3.1 Coincident $(e, e'\pi)$ Cross Section Model and Rate Estimate.

The model of coincident cross sections has the following inputs:

- The inclusive (e, e′) cross sections for protons and deuterons.
- A parameterization of fragmentation function $D^+(z)$ and $D^-(z)$ as functions of Q^2.
- A model of transverse momentum distribution of pions as fragmentation products.

The inclusive deep inelastic (e, e′) cross section can be expressed in the quark parton model as:

$$\frac{d^2\sigma}{d\Omega dE'} = \frac{\alpha^2(1+(1-y)^2)}{sxy^2}\frac{E'}{m_N\nu}\sum_i e_i^2\left(q_i(x,Q^2)+\bar{q}_i(x,Q^2)\right) \qquad (21)$$

where m_N is the nucleon mass, $y = \nu/E$, $s = 2Em_N + m_N^2$. The quark distribution functions $q_i(x, Q^2)$ and $q_{\bar{i}}(x, Q^2)$ are taken from the CTEQ5M global fits [7]. The predicted inclusive cross sections agree with SLAC data [14] to better than 20% within the kinematic region of this proposal.

The semi-inclusive $(e, e'h)$ cross section relates to the quark fragmentation function $\mathrm{D}_i^h(z, Q^2)$ and the total inclusive cross section σ_{tot} through:

$$\frac{1}{\sigma_{tot}} \frac{d\sigma(e, e'h)}{dz} = \frac{\sum_i e_i^2 f_i(x, Q^2) D_i^h(z, Q^2)}{\sum_i e_i^2 f_i(x, Q^2)}. \tag{22}$$

The two light quark fragmentation functions, $D^+(z, Q^2)$ and $D^-(z, Q^2)$, relate to each other roughly through [15]:

$$\frac{D^-(z, Q^2)}{D^+(z, Q^2)} = \frac{1 - z}{1 + z}. \tag{23}$$

The average pion fragmentation function $D^\pi(z, Q^2)$=1/2($D^+(z, Q^2) + D^-(z, Q^2)$) was parameterized (BKK parameterization) [16] based on fits of e^+e^- annihilation data. Existing data indicated that the fragmented products follow a nearly structureless azimuthal distribution and a Gaussian-like transverse distribution. For the $p(e, e'\pi^+)X$ reaction, at the kinematic point of $\nu = 4.10$ GeV, $W^2 = 4.56$ GeV^2 and Q^2=1.20 GeV^2, Bebeck *et al.* [17] determined that the pion transverse momentum ($p_\perp$) distribution follows the form of $e^{(-Bp_\perp^2)}$ with B=8.09 ± 0.65 GeV^{-2}, corresponding to a quark transverse momentum distribution of $\sigma_{p_\perp} = 0.25$ GeV. We used this pion distribution and realistic spectrometer acceptances in a Monte Carlo simulation to estimate the count rates. We note that when a virtual photon of several GeV strikes a quark, the majority of the fragmentation products remain within a few degrees of the direction of the virtual photon. Therefore, by detecting fragmentation products along the direction of $\vec{q}$, the Hall-A HRS spectrometer provides sufficient solid angle coverage. In this proposal, the kinematics are chosen such that the direction of $\vec{q}$ always lies within the acceptance of HRS.

With a 100 μA beam on a 15 cm standard Hall-A cryogenic hydrogen/deuterium target, the luminosity is 4.0×10^{38} cm^{-2}s^{-1}. The HRS spectrometer with the septum magnet has an angular acceptance of $\Delta\theta_{hor} = ^{+24}_{-19}$ mrad and$\Delta\theta_{ver} = \pm 50$ mrad, and a momentum acceptance of $\pm 4.5\%$ [18]. The well-collimated Big Bite setup as electron detector will accept at least 60% of the charged particles over a momentum range of $\pm 20\%$ within $\Delta\theta_{hor} = \pm 50$ mrad and $\Delta\theta_{ver} = \pm 50$ mrad. An electron detection efficiency of 90% is assumed. To test the onset of Generalized Factorization, we take six different P_π settings at Kinematics-1 and -2, and three P_π settings at Kinematics-3. The beam time arrangements at each settings are chosen such that the absolute value of r_1 can be determined to $\delta r_1 = 1.25\%$ statistically. The time distribution within one setting is chosen such that the yields from hydrogen and deuterium are measured with similar relative accuracies and yields of $\pi+$ and π^- are measured with similar absolute accuracies. The statistical uncertainty of r_2 is roughly half of the uncertainty of r_1, with the planned arrangement we have $\delta r_2 = 0.46\%, 0.53\%$ and 0.61% for each setting in Kinematics-1, -2 and -3, respectively.

The estimated count rate and beam time allocation in each setting are listed in Table 2. The beam time request is summarized in Table 3. In addition to the

476 hours of production beam time, we request 8 hours for a dummy target yield check, 12 hours for Hadron-arm magnetic filed changes For two angle changes of the electron arm, we request 16 additional hours of time, possibly it can be arranged during scheduled maintenance periods. Since the planned Big Bite detector package will not be used in other Hall-A approved experiments, some beam time should be available for parasitic developments. Additional Hall-A facility development time ($\sim$ 48 hours) will be requested separately for Big Bite calibrations and detector shakedown. A total of 512 hours (21 days) of beam time is requested for this experiment.

Table 2: Count rate estimates and beam time for each kinematic setting.

Label	z	P_π	Rate (Hz)				Time (Hours)				Time
			$R_p^{\pi^+}$	$R_p^{\pi^-}$	$R_D^{\pi^+}$	$R_D^{\pi^-}$	$T_p^{\pi^+}$	$T_p^{\pi^-}$	$T_D^{\pi^+}$	$T_D^{\pi^-}$	Sum
K1a	0.35	1.73	37.45	18.03	79.05	38.06	2.3	1.1	1.1	0.5	5.0
K1b	0.41	2.03	37.34	15.62	78.82	32.98	2.5	1.0	1.2	0.5	5.2
K1c	0.47	2.33	36.22	13.06	76.47	27.57	2.8	1.0	1.3	0.5	5.6
K1d	0.53	2.62	34.17	10.50	72.14	22.16	3.2	1.0	1.5	0.5	6.2
K1e	0.59	2.92	31.27	8.06	66.01	17.02	3.8	1.0	1.8	0.5	7.0
K1f	0.65	3.22	27.59	5.85	58.24	12.35	4.6	1.0	2.2	0.5	8.2
							Kin-1 Sub-Total: 37.0				
K2a	0.35	1.78	7.71	3.71	15.05	7.25	6.8	3.3	3.5	1.7	15.2
K2b	0.41	2.09	7.23	3.03	14.13	5.91	7.9	3.3	4.0	1.7	16.9
K2c	0.47	2.40	6.65	2.40	12.99	4.68	9.3	3.4	4.8	1.7	19.2
K2d	0.53	2.70	5.97	1.83	11.65	3.58	11.3	3.5	5.8	1.8	22.3
K2e	0.59	3.01	5.21	1.34	10.17	2.62	13.9	3.6	7.1	1.8	26.5
K2f	0.65	3.31	4.39	0.93	8.57	1.82	17.8	3.8	9.1	1.9	32.7
							Kin-2 Sub-Total: 133.0				
K3a	0.35	1.89	0.90	0.43	1.62	0.78	38.2	18.4	21.0	10.1	87.7
K3b	0.41	2.21	0.81	0.34	1.48	0.62	45.8	19.2	25.3	10.6	100.8
K3c	0.47	2.54	0.73	0.26	1.32	0.48	55.8	20.1	30.8	11.1	117.7
							Kin-3 Sub-Total: 306.0				
	Total Beam Hour:										476.0

4 Expected Results

Since we plan to measure yield ratios rather than the absolute cross section, sensitivity to instrumental effects are minimized. The major concern of systematic uncertainties comes from the possible bias between π^+ and π^- detection efficiencies and in luminosity corrections. Since we planned enough overlap on different pion momentum settings, local detection efficiency differences could be monitored

Table 3: Summary of beam time request.

	E' GeV	θ_e degree	Time (Hours)
Kin-1	1.05	25.50	37.0
Kin-2	0.90	37.50	133.0
Kin-3	0.60	59.50	306.0
Dummy Target Coincident Yield Check			8.0
Magnetic Field Changes and Target Moves			12.0
Electron Arm Move			16.0
Data Production Beam Time			512.0
Total Time Requested			512.0 (21 days)

and corrected. Luminosity monitoring through beam charge and target density measurement as well as spectrometer single events rates can correct the overall luminosity to 0.5% level. The difference in luminosity determination between π^+ and π^- measurements should be less than 0.25%.

The radiative correction differences between $(e, e'\pi^+)$ and $(e, e'\pi^-)$ reaction could introduce systematic uncertainties in extracting quark and anti-quark distribution ratios. We expect this kind of higher order radiative correction difference to be relatively small in the yield ratios. In principle, this correction can be calculated exactly in the frame work of QED. Although we are not aware of such a calculation at the moment, we certainly believe that a reliable procedure of radiative corrections in $(e, e'\pi^{\pm})$ reaction can be developed in the future.

Another issue in the interpretation of this experiment is the effects of final state interaction in $H(e, e'\pi)$ and $D(e, e'\pi)$ reaction. We intentionally chose pion momentum to be higher than 1.75 GeV/c for reduced $\pi - N$ scattering cross section to avoid complications of final state interaction. We also chose to avoid resonance region by taking W'^2 as high as possible ($3.5 < W'^2 < 6.1$ GeV^2) and observing the pions directly along the momentum transfer. Thus we expect the effects of final state interaction to be rather small. We are actively seeking help from theoretical colleagues on calculations regarding this issue.

We will have enough data to determine the onset of the generalized factorization to 1.25 % on r_1 and 0.5% on r_2. If a clear z-independent behavior is reproduced as in the HERMES experiment, the yield ratios will directly be the quark distribution ratios as $r_1 = (d + \bar{d})/(u + \bar{u})$ and $r_2 = (d - \bar{d})/(u - \bar{u})$. Strong constraints can be made to the quark distribution functions over the measurement region.

On the other hand, our measurements could demonstrate a transition to the factorization regime, with some kinematics show the evidence of factorization while others won't. A clear demonstration of such a transition will be very interesting. Lastly, if the evidence of generalized factorization cannot be identified through our

measurements, a clear contradiction to the HERMES data will be established. This will cast doubt on the usual methods of extracting quark distribution functions and quark spin distributions in deep inelastic semi-inclusive experiments.

4.1 Expected results on light quark and anti-quark distribution ratios.

The projected data on r_1 and r_2 measurements are shown in Fig. 12. The error bars on the data points are statistical only. In comparison to the projected r_1 data points we show in Fig. 13 a QCD fit result [19] of $(d+\bar{d})/(u+\bar{u})$. We point out that the typical deviation among different fit models differ by 3-10% in the region of $0.1 < x < 0.4$.

The projected data points of $\bar{d}/\bar{u}$ is shown in Fig. 14 together with Fermilab E866 and CERN NA51 data points.

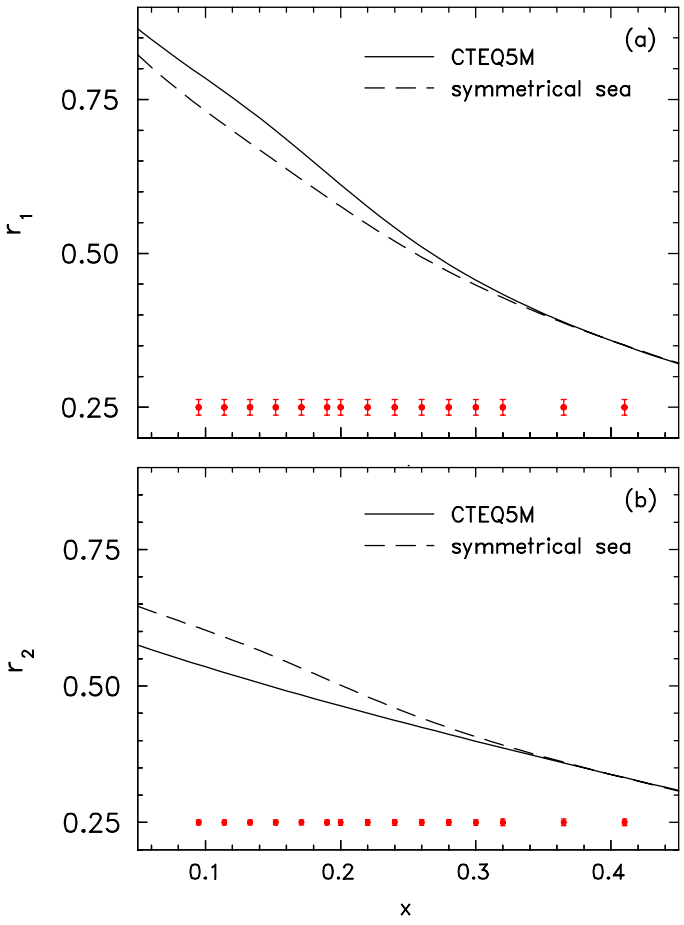

Figure 12: The projected data on r_1 and r_2.

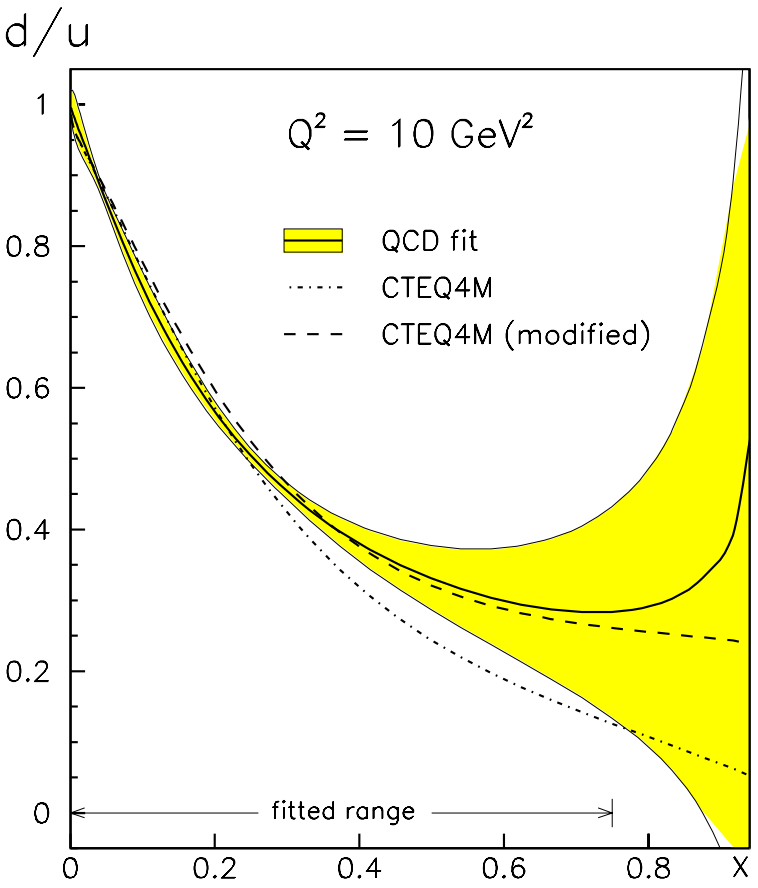

Figure 13: The ratio of $r_1 = (d + \bar{d})/(u + \bar{u})$ versus x at Q^2=10 GeV^2 from different fits. The solid line and the shaded band are QCD fits and error from M. Botje. Dashed-dotted curve is from CTEQ4M, and the dashed curve corresponds to CTEQ4M prediction with a modified down quark density.

4.2 Other possible physics products.

We note here that $(e, e'K^+)$ and $(e, e'K^-)$ events will also be collected in the data. Time of flight difference and PID provided by aerogel Cherenkov will be sufficient enough to separate them from $(e, e'\pi^\pm)$ events. Distributions of s-quarks could be accessed through this reaction.

Although we are not planning to measure the absolute cross sections with high precision, in principle, there is no obstacle to determining the absolute detector efficiencies and spectrometer acceptances at the $\pm 5\%$ level. Therefore, inclusive (e, e') cross sections, single pion cross sections, as well as π^+/π^- cross section ratios can also be determined. Extraction of fragmentation functions within our acceptance are also possible. It will be rather interesting to compare them with parameterization from high energy data.

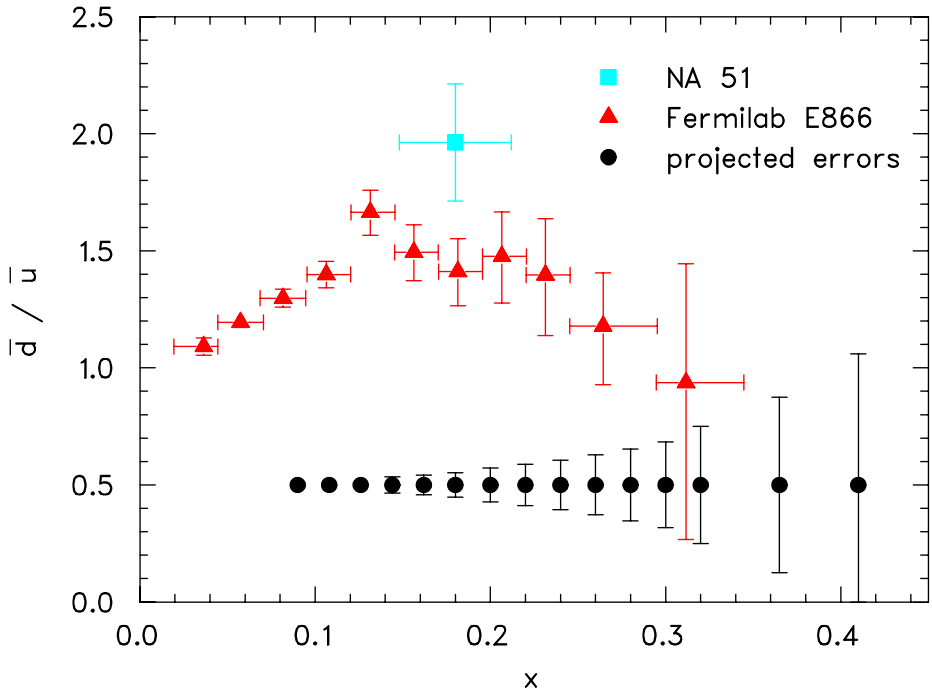

Figure 14: The projected data on $\bar{d}/\bar{u}$, statistical errors only.

5 Relation to Other Experiments

With luminosity of $(1-5)\times 10^{32}$ cm^{-2}s^{-1} for unpolarized beam at HERMES, six orders of magnitude lower than this proposal, it will be very time consuming to collect data to the same statistical accuracy as we proposed here. In addition, for a large detector setup as in HERMES, detection efficiency control at different part of the detectors to a precision of 0.5% level would prove to be very challenging.

Fermilab P906 is a proposed extension of Fermilab fixed target E866 experiment using a high intensity 120 GeV proton beam out of the Fermilab Main Injector. The P906 proposal would increase the x coverage to 0.45 with much improved statistics over E866 data. Using the completely different Drell-Yan ratio technique, P906 is not in competition with this proposal.

Very small forward angle access is almost impossible in Hall C and Hall B. This fact makes the deep-inelastic semi-inclusive reactions, such as in this proposal, inaccessible to these two Halls at 6 GeV energy without an extensive hardware development efforts. We note that Hall-C proposal PR-00-004 (C. Armstrong . *et al.* PAC-17) was proposed to test "Duality in Meson Electroproduction" using the $(e,e'\pi)$ reaction, however, we do not share the same physics goals, measurement techniques, and kinematics.

6 Summary

In conclusion, we will be able to make high precision measurements of deep inelastic semi-inclusive π^+/π^- yield ratios on hydrogen and deuterium to test the generalized factorization and to extract light quark and anti-quark distributions ratios. JLab at 6 GeV will allow us to reach W^2 high enough such that deep inelastic scattering measurements become possible. At a higher x range and much better statistical precision than the HERMES experiment, we will be able to independently test the Fermilab E866 results with a completely different reaction mechanism. If proven successful, this method would allow us to extend the measurements to quark spin density distributions and to strange-sea quark distributions. A total of 512 hours of beam time is requested for experiment with 6 GeV unpolarized beam in Hall-A.

Acknowledgments

We would like to thank Prof. W. Melnitchouk and Prof. F. Olness for many helpful discussions.

References

1. K. Gottfried, *Phys. Rev. Lett.* **18**, 1174 (1967).
2. P. Amaudruz, *et al.*, *Phys. Rev. Lett.* **66**, 2712 (1991).
3. F. M. Steffens and A. W. Thomas, *Phys. Rev.* C **55**, 900 (1997), S. Kumano, Phys. Rep. Vol. 303, 4(1998) pp183-257.
4. S. D. Ellis and W. J. Stirling, *Phys. Lett.* B **256**, 258 (1991),
5. J. Levelt *et al.*, *Phys. Lett.* B **263**, 498 (1991),
6. E. A. Hawker, *et al.*, *Phys. Rev. Lett.* **80**, 3715 (1998).
7. H. L. Lai, *et al.*, *Phys. Rev.* D **55**, 1280 (1997).
8. A. D. Martin, R. G. Roberts, and W. J. Stirling, *Phys. Lett.* B **387**, 419 (1996),
9. J. C. Peng, *et al.*, *Phys. Rev.* D **58**, 092004 (1998).
10. M. Glück, *et al.*, *Z. Phys.* C **67**, 433 (1995).
11. W. Melnitchouk, *et al.*, *Phys. Lett.* B **435**, 420 (1998).
12. B. Wojtsekhowski, C. Hyde-Wright and A. Nathan, JLab proposal E99-114, (1999).
13. J. W. Lightbody, Jr. and J. S. O'Connell, Computers in Physics, 1988
14. L. W. Whitlow, SLAC-Report-357, March (1990).
15. R. D. Field and R. P. Feynman, *Nucl. Phys.* B **136**, 1 (1978).
16. J. Binnewies, B. A. Kniehl and G. Kramer, *Phys. Rev.* D **52**, 4947 (1995).
17. C. J. Bebek, *et al.*, *Phys. Rev. Lett.* **30**, 624 (1973).
18. J. LeRose, private communication, and Hall-A Hypernuclear Collaboration, Technical Notes on Septum Magnets Design, September (1996).
19. M. Botje, hep-ph/9912439.